

Non-planar four-mirror optical cavity for high intensity gamma ray flux production by pulsed laser beam Compton scattering off GeV-electrons

J. Bonis^a, R. Chiche^a, R. Cizeron^a, M. Cohen^a, E. Cormier^b, P. Cornebise^a, N. Delerue^{a*}, R. Flaminio^c, D. Jehanno^a, F. Labaye^a, M. Lacroix^a, R. Marie^a, B. Mercier^a, C. Michel^c, Y. Peinaud^a, L. Pinard^c, C. Prevost^a, V. Soskov^a, A. Variola^a and F. Zomer^a

^a*Laboratoire de l'Accélérateur Linéaire, CNRS-IN2P3 Université Paris-sud 11 ,
15, rue Clémenceau, F-91898 Orsay Cedex, France*

^b*CELIA, CNRS, Université Bordeaux 1 ,
43 rue Pierre Noailles, F-33405 Talence, France*

^c*LMA, CNRS-IN2P3 Université Lyon 1 ,
7, Avenue Pierre de Coubertin, F-69622 Villeurbanne Cedex, France
E-mail: delerue@lal.in2p3.fr*

ABSTRACT: As part of the R&D toward the production of high flux of polarised Gamma-rays we have designed and built a non-planar four-mirror optical cavity with a high finesse and operated it at a particle accelerator. We report on the main challenges of such cavity, such as the design of a suitable laser based on fiber technology, the mechanical difficulties of having a high tunability and a high mechanical stability in an accelerator environment and the active stabilization of such cavity by implementing a double feedback loop in a FPGA.

KEYWORDS: Compton scattering; Fabry-Perot cavity; positron production; ATF; ILC; CLIC; Gamma rays; Compact Light Source.

*Corresponding author.

Contents

1. Introduction	1
2. The Optical system	3
2.1 Requirements	3
2.2 High average power low phase noise laser system	4
2.3 High finesse Fabry-Perrot cavity	6
3. Mechanical design and construction	9
3.1 Requirements for the mechanical design	9
3.2 Description of the mechanical system	10
4. Fabry-Perot Cavity stabilization and the electronic system	15
4.1 FPC synchronization with the accelerator	16
4.2 Oscillator synchronization with the FPC	18
5. Performances and future developments	23

1. Introduction

Recent results in cultural heritage conservation [1], medicine [2, 3, 4], nuclear [5, 6] and particle physics [7, 8, 9] have shown that there is a strong interest in producing high X and γ ray fluxes by Compton scattering a laser beam onto an electron beam.

Two ambitious projects are starting [10, 11] to provide a compact monochromatic X-ray source [12] from the scattering of a laser beam on electrons with an energy in the 10 – 100MeV range for medical imagery and heritage applications. Because of the small Compton cross section, a laser beam average power between 100kW and 1MW is needed.

At high energy, in the context of the linear collider projects CLIC[13] and ILC[14], the gamma rays produced by Compton scattering of a circularly polarized laser beam on a few GeV electron beam can be used to create a longitudinally polarized positron beam [7, 8, 15] or high energy gamma beams [9]. Nevertheless, this application of Compton scattering requires a huge laser beam average power above the Megawatt level.

The technology to reach the extremely high average laser power required for these applications is not yet mature. Direct amplification technology is highly inefficient and does not stand large average power (see e.g. [16]). Instead the use of an optical resonator [17], *i.e.* a Fabry-Perot cavity (FPC), of very high finesse filled with a pulsed laser beam [18, 19] allows to reach a high power at the collision point with easier requirements on the amplification and a much higher efficiency. If the electron beam passes inside the FPC one can indeed benefit from the power gain, defined by

the finesse over π , of the resonator provided that resonance conditions are fulfilled. However, a strong feedback is needed to lock a mode lock laser beam to a FPC [20]. In optical laboratories, a stored average power of $\simeq 70\text{kW}$ was achieved recently [21] and the operation of cavity finesse of $\simeq 30000$ was demonstrated [22]. In accelerator environments very few experiments have been carried out. In continuous regime, a cavity finesse of $\simeq 30000$ has been operated routinely [23, 24] and in the pulsed regime cavities of finesse $\simeq 3000$ on a short linear accelerator [25] and $\simeq 1000$ on the ATF ring [26] have been operated.

In order to increase the Compton γ -ray flux one must not only increase the stored laser pulse power but also reduce the waist of the cavity mode. It is well known [17] that two-mirror cavities become unstable when the mode waist decreases and that four mirrors, or more, must be considered in this case (see [27] for example). All resonators having been operated in accelerators up to now were made of two mirrors.

In this article, we describe a new experimental apparatus installed at the KEK ATF [28] that will contribute to a global R&D effort to reach the 100kW level of stored average power inside a four-mirror cavity. A new, non-planar geometry is used for the first time to provide highly stable and circularly polarized cavity eigenmodes [27]. The results reported here are those obtained with our apparatus before the earthquake that struck Japan in March 2011 and therefore we expect to be able to improve them once the apparatus will have fully recovered and be ready for operations again.

The ATF damping ring at KEK [28, 29] operates at a frequency of 357MHz and a round trip in the ring takes 462ns (there are 165 RF buckets spaced by 2.8ns). Up to 3 trains of 10 bunches separated by 5.6ns can be injected in the ring however most operations are done with a single bunch in the ring. Our FPC is installed in one of the straight sections of the damping ring as shown on figure 1.

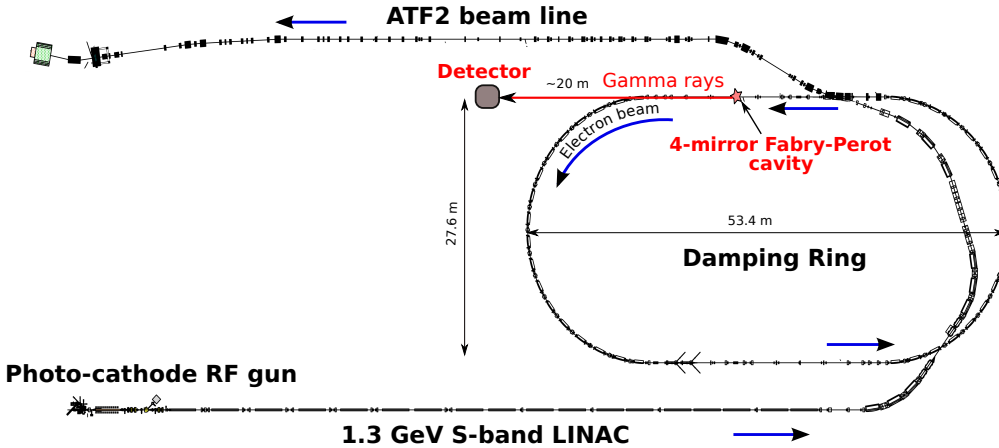


Figure 1. The Accelerator Test Facility (ATF) at KEK. The green box indicates the approximate locate of the 4-mirror cavity described in this paper. The red arrow indicates the direction of travel of the gamma ray produced. The blue box indicates the gamma-ray detector (adapted from [29]).

The laser oscillator that can be locked to a very high finesse cavity must exhibit the smallest possible phase (or frequency) noise. Such oscillator deliver typically only an average power of about 100mW. Even with a cavity finesse of $\simeq 30000$ and a perfect laser beam/cavity mode coupling one could only reach $\simeq 1\text{kW}$ average power inside the cavity. A laser amplification stage, designed to reach high average power without contributing too much additional frequency noise, is therefore also needed to meet the performance requested for the applications mentioned above. In addition, the laser beam must be circularly polarized for the polarized positrons source application.

To reach a high incident average laser power, we choose to use an Yb doped photonic fiber chirp pulse amplifier. This recent technology is very promising, at present $\approx 800\text{W}$ average power were obtained with a 78 MHz repetition rate, 640 fs pulse time width laser beam [30]. The long term stability and reliability are however still crucial issues and remain to be demonstrated. In this article, we report, for the first time to our knowledge, on the operation of a 50W amplifier installed close to the FPC in the ATF accelerator.

The mechanical design of the cavity includes a Compton scattering interaction point and fulfills the strong requirements set by the ATF accelerator. These stringent requirements lead us to develop new high precision mirror mounts for ultra high vacuum.

We implemented the Pound-Drever-Hall (PDH) laser/cavity feedback method [31] using a fully numerical system based on a field programmable gate array (FPGA). FPGAs have already been used in a recent past to lock laser oscillators to reference frequencies. In addition, the relatively easy programming of the feedback filters and integrators offers a flexibility that helps to perform the complex locking of a laser frequency comb [32] to a cavity [33, 34]. However, an analog part is still often included either in the feedback system or for the measurement of the response functions required to tune the feedback. The system presented in this article contains, for the first time to the authors' knowledge, all the feedback bricks inside the FPGA, that is the frequency modulation/demodulation, the error signal filtering, the production of the correction signals and the identification procedure leading to the response functions.

The commissioning of our apparatus at the ATF has been successfully done during winter 2010-2011. Since many new experimental features have been developed to build the experimental setup, the present article is solely devoted to the apparatus. The first results obtained during the commissioning, before the earthquake of March 2011, are published in a companion article [35].

This article is organized as follows. In section 2 the optical system, the laser amplification and the FPC are described. The mechanical system is discussed in 3. The electronic and the feedback system are presented in section 4.

2. The Optical system

2.1 Requirements

To deliver a beam suitable for injection in the FPC the seed laser oscillator must provide a frequency comb in frequency space [32] with an extremely stable repetition rate f_{rep} and Carrier-Envelope Phase (CEP). The comb teeth are defined by [32, 20]:

$$\nu_n = \left(n + \frac{\Delta(\phi_{ce})}{2\pi} \right) f_{rep}$$

where f_{rep} is the laser pulse repetition rate (178.5 MHz in our case); $n \approx 10^6$ is an integer number; $\Delta(\phi_{ce})$ is the carrier-envelope phase variation between two successive laser pulses. From this expression one can see that to lock a full frequency comb to a FPC, one must control two different parameters f_{rep} and $\Delta(\phi_{ce})$. It was shown that the PDH method [31, 36] can provide error signals as requested to perform the laser beam / FPC synchronisation [33, 34]. In practice the dispersion induced by the propagation inside the cavity mirror coatings limits the number of combs that can be locked to a FPC and introduces some coupling losses [37]. In our setup, the width of the incident laser beam spectrum is reduced to 2 nm (see section 2.2). We computed the variation of the cavity power coupling as a function of $\Delta(\phi_{ce})$. Assuming that f_{rep} is locked to a FPC round trip and a finesse of 3000, we obtained an expected maximum power coupling loss of $\approx 35\%$ for $\Delta(\phi_{ce}) \in [0, 2\pi]$ and $\approx 90\%$ for a 30000 FPC finesse. In the present article, a 3000 cavity finesse is used and no attempt was made to control $\Delta(\phi_{ce})$.

Another important feature of the FPC behavior in pulsed regime is the longitudinal mode structure. When the FPC length is detuned by $m\lambda$, where λ is the laser beam wavelength, secondary resonances with lower power coupling are observed [20]. In [38] it was shown that an effective cavity bandwidth can be defined and that, for a longitudinal resonance of order m , it increases with m . In our experiment we made use of this property by locking our FPC to the $m = 1$ resonance during the very first step of the commissioning at ATF before switching to the main resonance ($m = 0$).

As the power required to inject the passive FPC exceeds by far the output power of any low phase noise oscillator, the seed beam must be amplified in an optical amplifier. Here again, a special attention should be taken in designing the amplifier system as it should not add any phase noise to the seed beam in order to maintain a high coupling in the FPC and reach the theoretical FPC gain. The spatial quality of the amplified beam is also important to ensure an efficient coupling. Ideally it should optimally match the nearly perfect mode of the high finesse FPC.

Since the collision occurs at a slight angle (see the mechanical description in section 3 and in particular figure 6), the laser pulse duration must be close to that of the electron bunches, that is $\simeq 20$ ps in our case at ATF.

2.2 High average power low phase noise laser system

The laser architecture has been dictated by the optical parameters required for this experiment.

The laser system is based on a master oscillator power amplifier (MOPA) implementing a chirp pulse amplification (CPA) scheme in Yb-doped diode pumped fiber. It consists of a customized commercial oscillator (Origami-10 from Onefive GmbH) delivering transform-limited 200 fs sech pulses at a wavelength around 1030 nm and at a repetition rate of 178.5 MHz (to match half the bucket of the DR). Because we make use of a fiber amplifier, amplification of short pulses in a reduced diameter long waveguide may induce nonlinear effects as the intensity in the fiber glass grows. The present experimental setup and more specifically the external cavity enhancement of the laser pulses simply can't suffer from any non-linearities. In fact accumulating non-linear effect during the beam propagation may result in amplitude-to-phase coupling potentially ruining the locking procedure to the FPC. Therefore, to reduce intensity in the gain medium, the pulses are temporally stretched before amplification and recompressed after in the so-called CPA architecture. In order to keep the system as compact as possible, temporal stretching is performed by propagating

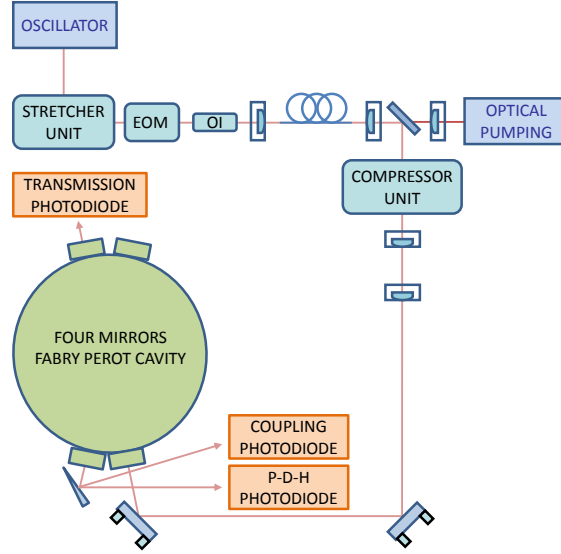


Figure 2. Optical system including a frequency comb oscillator, a fiber amplifier and a FPC.

the beam in a chirped volume Bragg grating (CVBG [39]) supplied by Optigrate. The principle of CVBG relies on the fact different wavelengths are reflected at different depth in the bulk grating inducing a time delay between consecutive wavelengths of the spectrum. By properly engineering the Bragg structure recorded in the bulk material, it is possible to define a well controlled dispersion law. In our case the dispersion is mainly of second order and stretches the initial 200 fs pulses to more than 200 ps. The CVBG also act as a filter as its transmission bandwidth is much more narrow than than the oscillator bandwidth. This is depicted on figure 3 where we superimpose the oscillator spectrum (5 nm) with the reflected spectrum (2.2 nm). The pulse length required for the Compton scattering in our configuration are of the order of several tens of ps and therefore perfectly compatible with spectral filtering. Note here that filtering should not be too important to allow sufficient stretching. The global efficiency of the stretcher unit is about 37.5 % mainly due to the filtering process [39].

The stretched beam is then propagated through an electro-optic modulator set for phase modulation and driven by a 5 MHz RF signal necessary to generate the error signal for the PDH locking system described in section 4. In order to prevent any artificial noise generation and locking degradation from backscattered light, the laser oscillator is isolated from the rest of the system and in particular from the amplifier with a double Faraday isolator having an extinction ratio of 56 dB. At this point, the beam is injected in the fiber amplifier. The amplifier consists of a 2-meter long double clad Yb-doped photonic crystal fibre with a 40 μm core diameter and a 200 μm cladding diameter (NKT DC-200/40-PZ-Yb supplied by NKT Photonics). The fiber is end-pumped by a high-power laser diode (supplied by DILAS). The output power varies linearly with the pump power with a

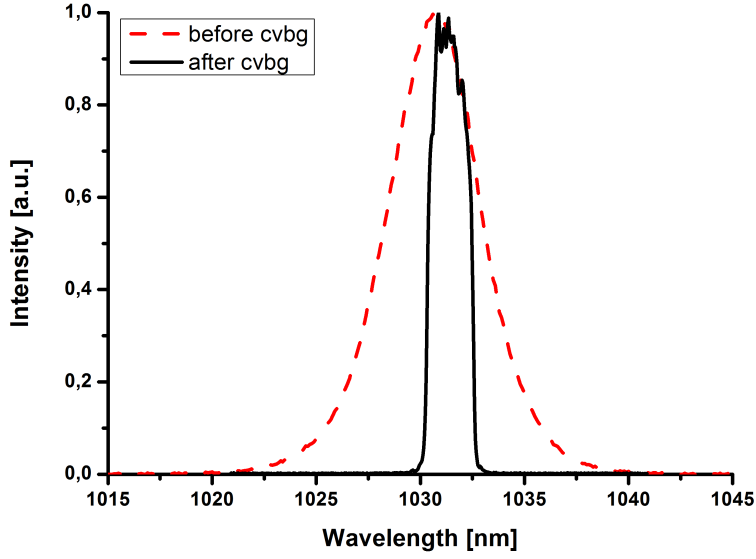


Figure 3. Spectra of the laser beam measured before and after the CVBG

slope efficiency of 51% as shown on figure 4. A maximum output power of 55 W was achieved with this setup. The beam quality is of major importance in the present context as any deviation from a perfect Gaussian beam will be rejected by the high finesse FPC and will not contribute to the power accumulation inside the FPC. This is one of the reason why we have chosen amplification in a single mode active fiber. We measured an amplified beam quality $M^2 = 1.07$ (axe x) $M^2 = 1.07$ (axe y) in our laboratory. In figure 5 we give a typical intensity profile measured at 28 W output power after installation of our system at ATF. The beam is then sent in the compressor unit consisting of another CVBG. In order to adjust the final duration, the compressor CVBG might be different from the stretcher CVBG (still opposite sign but different value). In our case the minimal duration is not an objective. Instead, we are more interested in optimizing the duration of the laser pulse to match that of the electron bunch and maximize the gamma-ray production. In the present case, pulses are recompressed to 68 ps and therefore exhibit a large chirp due to the remaining second order dispersion. The chirp has no effect on the gamma production nor on their characteristics.

Finally, the beam is propagated through an arrangement of lenses carefully chosen to optimally match the FPC mode at injection.

2.3 High finesse Fabry-Perrot cavity

As mentioned in the introduction, two-mirror cavities are unstable for small mode waist sizes. To address this issue and others we choose to use a four-mirror cavity instead. In order to provide stable circularly polarized eigenmodes (as required by high energy physics [7, 8]), a non-planar tetradron geometry is chosen [27] as shown in figure 6. The cavity is made of two concave mirrors, M_3 and M_4 of radius of curvature 0.5m and of two flat mirrors M_1 and M_2 . The cavity

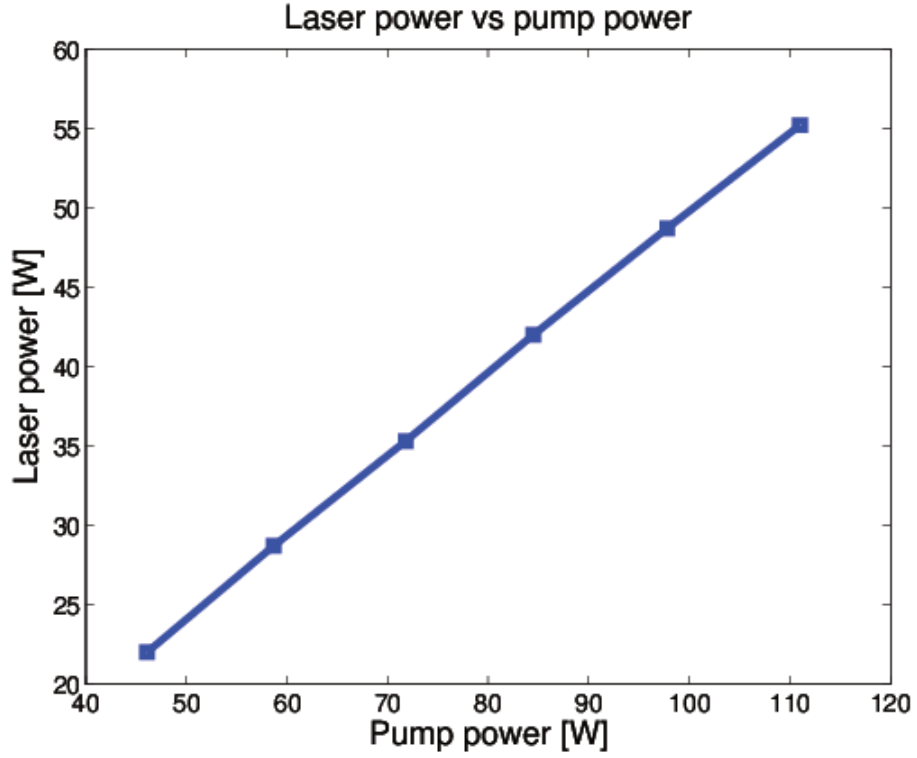


Figure 4. Efficiency curve of the Yb-doped fiber amplifier.

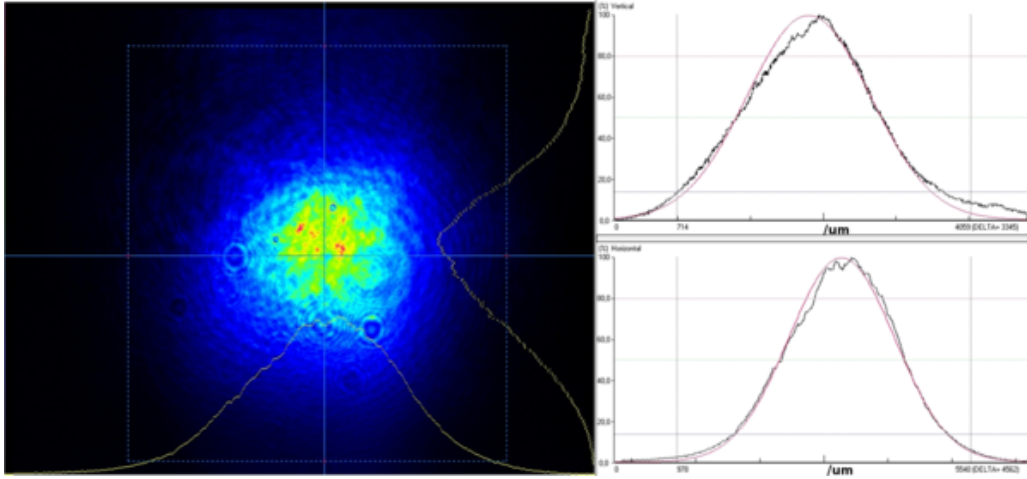


Figure 5. Spatial intensity profile at the output of the fiber amplifier at 28 W output power

finesse is determined by the reflection coefficients r_i of the mirrors M_i which depend themselves on the number of $\text{SiO}_2/\text{Ta}_2\text{O}_5$ double layers deposited on the mirror substrate. In order to optimize the laser/cavity mode coupling, we fixed $r_1 \approx r_2 r_3 r_4$ [40], where M_1 is the entrance cavity mirror. For the cavity commissioning we choose $|r_2|^2 \approx |r_3|^2 \approx |r_4|^2 \approx 1 - 330\text{ppm}$ and $|r_1|^2 \approx 1 - 1060\text{ppm}$

leading to a finesse $F = \pi/(1 - |r_1 r_2 r_3 r_4|) \approx 3000$ (*i.e.* a power gain of $G = F/\pi \approx 1000$). The mirrors coating were made by ourselves at the LMA Laboratory of Lyon. In the finesse expression given above, the losses [40] are neglected, this is justified because we have measured the absorption and the scattering of the mirror coating to be $\approx 0.6\text{ppm}$ and $\approx 3\text{ppm}$ respectively.

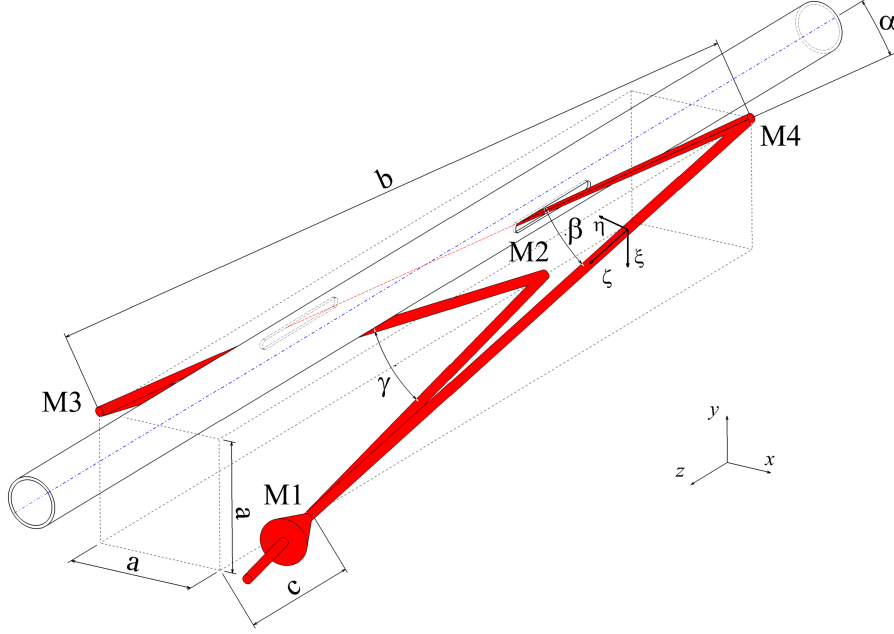


Figure 6. Schematic drawing of the four-mirror cavity installed at ATF. The laser beam is represented by the red lines and the incident laser beam by a red arrow. A rectangle parallelepiped, defined by $a = 70\text{mm}$ and $b = 500\text{mm}$ is drawn as a guide line. The spherical mirrors M_3 and M_4 are located in the vicinity of two of the corners of the parallelepiped. The two flat mirrors are shifted by $c \approx 81.19\text{mm}$ along the bottom line segments M_1 and M_2 . The beam pipe and the rectangular slit of 5mm large is shown as well as the fixed reference frame (x, y, z) and the frame attached to the laser beam optical path (ξ, η, ζ) . $\alpha = 8.05^\circ$ is the laser beam/electron beam crossing angle and $\beta/2 = 6.25^\circ$, $\gamma/2 = 7.6^\circ$ are the two incident angles on M_2 (and M_1) and M_4 (and M_3) respectively.

The mirror positions (see figure 6) are chosen such that the cavity round trip optical path matches the distance between two electron bunches of the ATF, that is $\approx c/178.5\text{MHz} \approx 1.681\text{ m}$. The FPC being non-planar, the eigenmodes belong to the class of general astigmatic beam [41, 42], that is the intensity spatial profile is an ellipse with principle axes rotating during the propagation (see [43] for a tetrahedron cavity). The distance between the spherical mirrors is tuned in order to provide a cavity mode waist sizes of $52\mu\text{m}$ and $76\mu\text{m}$ (*i.e.* equivalent Gaussian intensity spot radii of $26\mu\text{m}$ and $38\mu\text{m}$) half way between the two spherical mirrors. With such beam radii, diffraction losses induced by the beam pipe slit aperture (see section 3) are negligible. Figure 7 shows the spatial beam profile measured behind M_2 . From this measurement, using the eigenmode calculation of [42] we can estimate the evolution of the beam size inside the cavity. The effect of the ellipse axis rotation was studied in [43], in our setup it also leads to negligible luminosity loss. We checked our calculations in a dedicated experiment where the cavity beam waist was imaged using an converging lens located in transmission on M_4 [44]. A good agreement was obtained. The

circular polarization of the eigenmodes were measured in [45]. We also checked numerically that, for the ATF electron beam parameters [28], the laser beam intensity profile rotation has a very small impact of the electron/laser beams luminosity [43]. We verified numerically and experimentally that varying the distance between the two flat mirrors within $\pm 2\text{mm}$, that is the dynamical range of the mirror longitudinal positioning system, the beam waist size does not change significantly. On the other hand, the beam waist size is very sensitive to the distance between the two spherical mirrors.

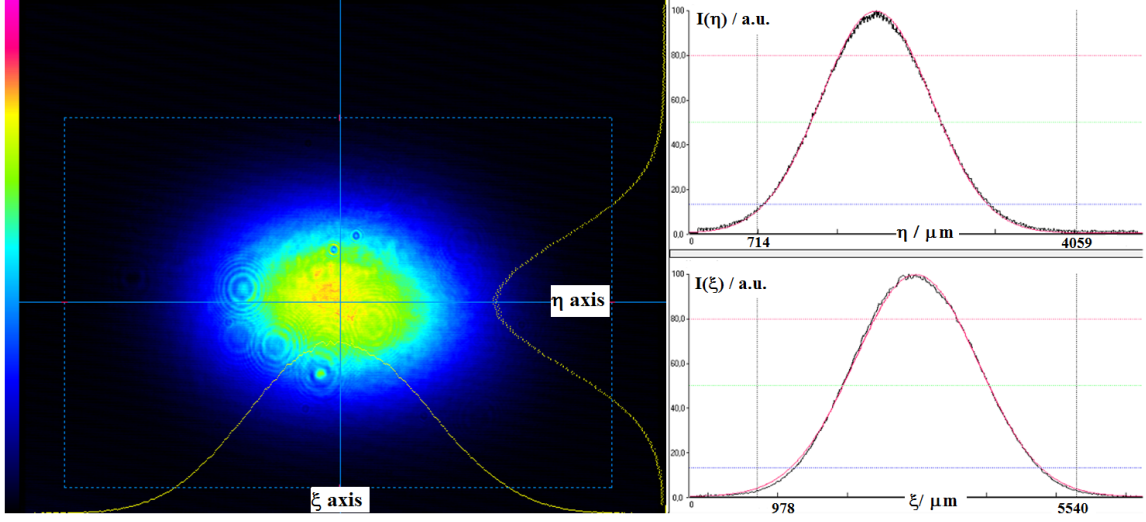


Figure 7. Typical beam intensity transverse profile $I(\xi, \eta)$ as measured by a laser beam scanner located just behind M_2 . The left plot shows the two dimensional as a function of the transverse coordinates ξ and η . The right plots show the projections along the principal axes ξ and η together with Gaussian fits. From these fits we obtain $\omega_\xi = 1.75\text{mm}$ and $\omega_\eta = 1.17\text{mm}$.

3. Mechanical design and construction

3.1 Requirements for the mechanical design

The strongest requirements on the design of a non planar cavity (see section 2) for Compton scattering come from its installation in an accelerator. As the ATF is one of the electron rings with the world's smallest transverse emittance [46] we had to minimize any perturbation on the electron beam by providing a sufficiently low vacuum (below 10^{-7}mbar) and by ensuring as little discontinuity as possible of the beam pipe impedance. The later point means that the beam pipe must continue inside the cavity. To allow the laser beam to cross the electron beam a slit had to be machined in the beam pipe. This slit has a vertical dimension of 5mm (see figure 6), the largest acceptable aperture from the ATF machine point of view. Such a small inner aperture requires the ability to tilt the cavity mirrors so that the laser beam can be steered through this aperture while being sufficiently immune to environmental noises. This must be achieved by using sub-micrometric actuators fixed on gimbal mirror mounts.

Since the laser beam is pulsed, the cavity round trip must coincide with the distance between two electron bunches at the ATF. Some of the mirrors must thus also be mounted on longitudinal

translation stages for a coarse tuning of the optical path and one of them must be connected on a piezo electric transducer to allow fine tuning (*i.e.* for the synchronization with the ATF clock, see section 4).

The 5mm beam pipe aperture slit fixes the divergence of the optical cavity mode, *i.e.* the laser beam waist size avoiding diffraction losses is limited and its minimum value is estimated to $\approx 35\mu\text{m}$. In order to optimize the luminosity it is then necessary to reduce the laser beam - electron beam crossing angle. The mirror mounts of the two spherical mirrors must then be designed in such a way to minimize the material budget between the mirror center and the beam pipe.

Finally, one needs to provide a high level of mechanical stability for the synchronization of the laser oscillator with the high finesse cavity. Special attention must thus be paid to the stability of the mirror mounting system and to the isolation of the whole optical system against thermal fluctuations and, ground and air induced vibrations.

3.2 Description of the mechanical system

Each mirror is mounted as described on figure 8. Three actuators allow to tilt the mirrors in x and y directions and to move them along the z axis. An exploded view of the tilting system is shown on figure 9. The mirrors are inserted in a ring fixed on a gimbal mount made of two flexible hinges. The hinges are machined by wire erosion-cutting of a stainless steel cube and the hinge motion results from the elasticity of the remaining thin material: one of the hinges can be tilted in the x direction and the other in the y direction while keeping the mirror center at the same location. To control the hinge tilts, two encapsulated stepper motors (see also the exploded view on figure 10) are connected to a triangular arm, itself fixed to the surface of the gimbal mount. Then a spring is used to constrain the system. Figure 10 shows that the motor motion is transmitted to the triangular arm through a small bellow and that a hard steel pellet is fixed at the end of the cap in order to reduce friction effects. The motor cap is filled with Helium through a small flange in order to identify possible leaks. For the minimum motor step $\pm 0.3\mu\text{m}$ we have measured a tilt of $\pm 2.7\mu\text{rad}$ of the mirror plane. The maximum motor excursion of $\pm 1\text{mm}$ therefore corresponds to a maximum tilt of $\pm 9\text{mrad}$. Figure 8 shows in fact the mounting system of one of the two spherical mirrors. The side cut of the mirror mount, leading to a reduced laser-electron beams crossing-angle, is clearly visible. For one of the flat mirrors, the ring was adapted to include an annular piezo electric transducer (see figure 9) constrained by a flexible ring made by wire erosion-cutting.

The longitudinal translation stage is shown on figure 8. The mirror mounting system is put on three ceramic balls guided by two tracks. The motion is also done thanks to an encapsulated motor. As shown on figure 11, the motors are fixed on an invar plate itself fixed by its center on a 65 kg stainless steel base plate in order to increase the stability of the mirror positions under thermal variations. A picture of the four-mirror system is shown in figure 12.

Finally the whole system is put inside a cylindrical vacuum chamber supplied by Caburn (MDC). Because of the complexity of the system no baking was done. Therefore all pieces were carefully cleaned and mounted inside the chamber in a class 10 clean room (*i.e.* ISO4) at LAL, Orsay, then sealed and sent to KEK. Once at the ATF, all manipulations inside the cavity were done under a class 100 (*i.e.* ISO5) clean laminar air flow. We measured the position of each element inside the chamber with an absolute precision of 0.2mm so that we were able to fix z position variation range of each mirror mounts to $\pm 1\text{mm}$.

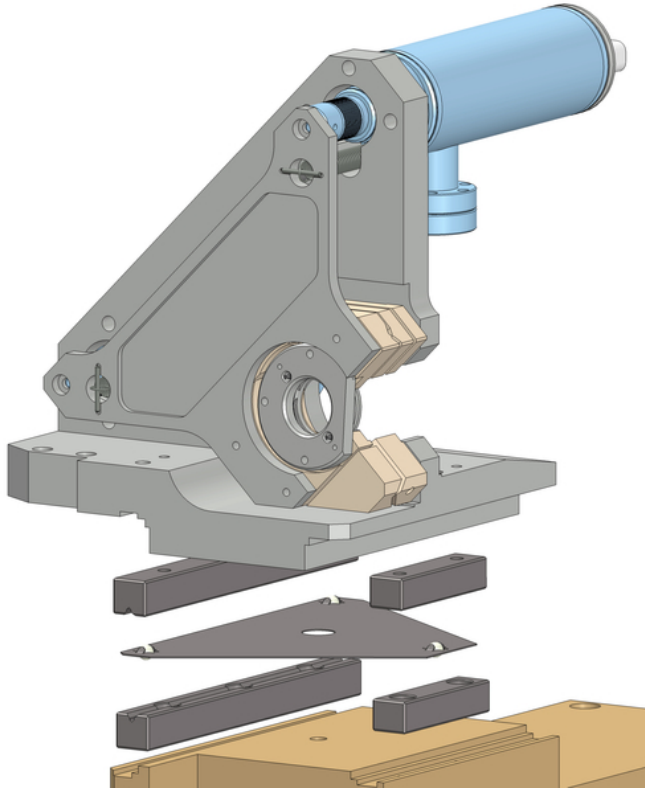


Figure 8. Technical drawing of a spherical mirror mounting system. The longitudinal translation stage, made of three ceramic balls, two guiding rails and a triangular plate is shown as an exploded view.

Because of the high vacuum requirements, all mechanical elements are made of stainless steel (and all screws and nuts are silver coated). The special gimbal mirror mount and the three ceramic balls system for the longitudinal motion are designed to avoid galling, making the mirror motion frictionless.

By using encapsulated motors inside the vacuum vessel we were able to decouple the tilt from the translation mirror motion and to reduce the effects of external noises. The equilibrium vacuum measured inside the cavity is about 3×10^{-8} mbar (≈ 30 m of high vacuum electrical wires are contained in the vacuum chamber) and no noticeable contamination from atoms with $Z > 18$ has been measured as specified by the ATF vacuum requirements and to preserve the high reflectivity of the cavity mirror coatings.

A set of isolators are used to reduce the effects of environmental noises: two bellows are located on each side of the vacuum chamber to align and isolate the system from the rest of the damping ring; three A5 aluminum feet inserted between the chamber and the optical table; and the optical table is standing on a dozen of elastomer bumpers. The optical table is enclosed in a box made of an acoustic insulating material and a system of heating wires is used to stabilize the temperature inside this box with a precision of $\pm 0.05^\circ\text{C}$.

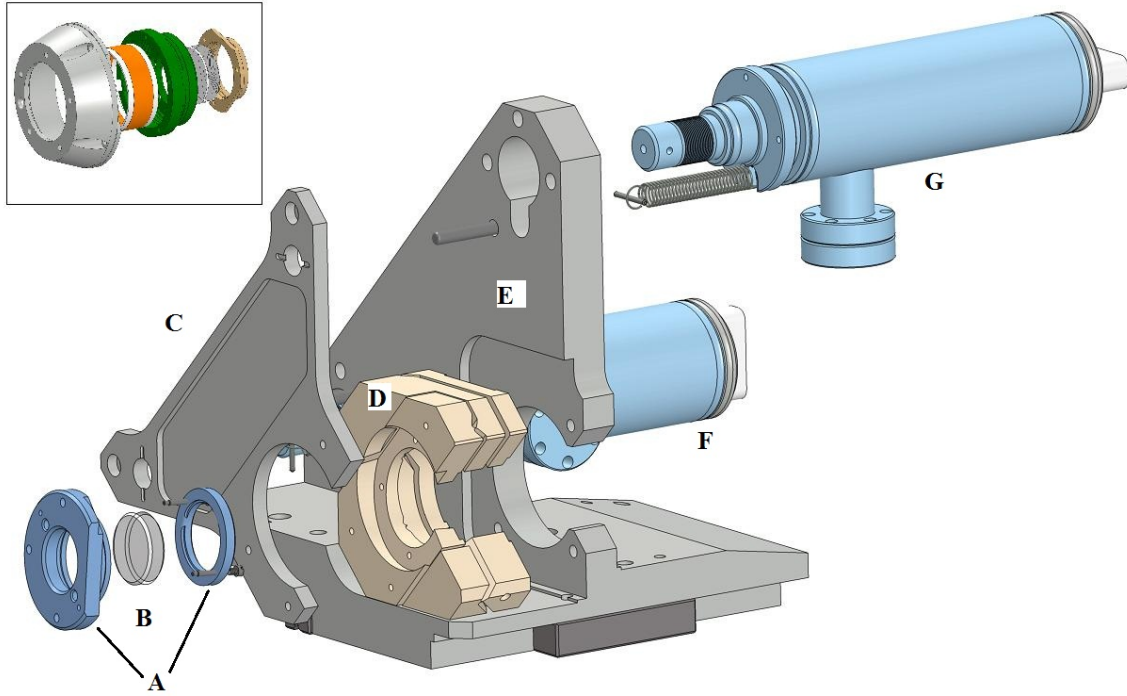


Figure 9. Exploded view of the tilt system. A: mirror ring system; B: cavity mirror; C: triangular arm; D: gimbal mirror mount; E: mirror mount support; F: encapsulated motor for actuating the rotation along the x horizontal axis; G: encapsulated motor for actuating the rotation along the y vertical axis. On the top left of the figure, the mirror ring containing the annular piezoelectric transducer (represented by an orange cylinder) is also shown.

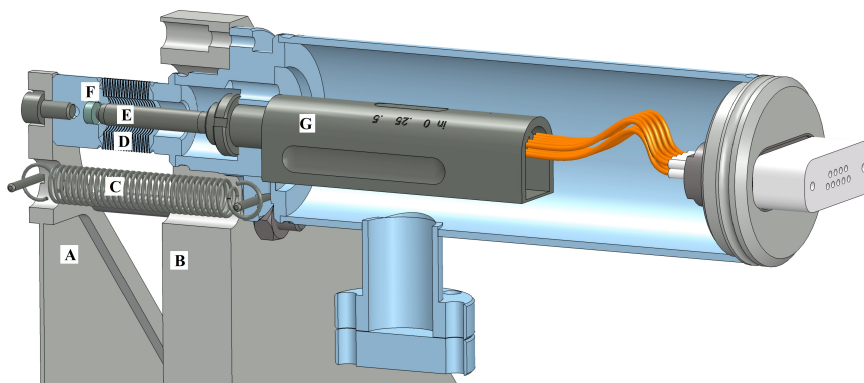


Figure 10. Cut view of the encapsulated commercial stepper motor. A: triangular arm; B: mirror mount base; C: spring; D: small bellow; E: stepper motor screw; F: hard steel pellet used to avoid friction of the end of the motor screw; G: stepper motor body.

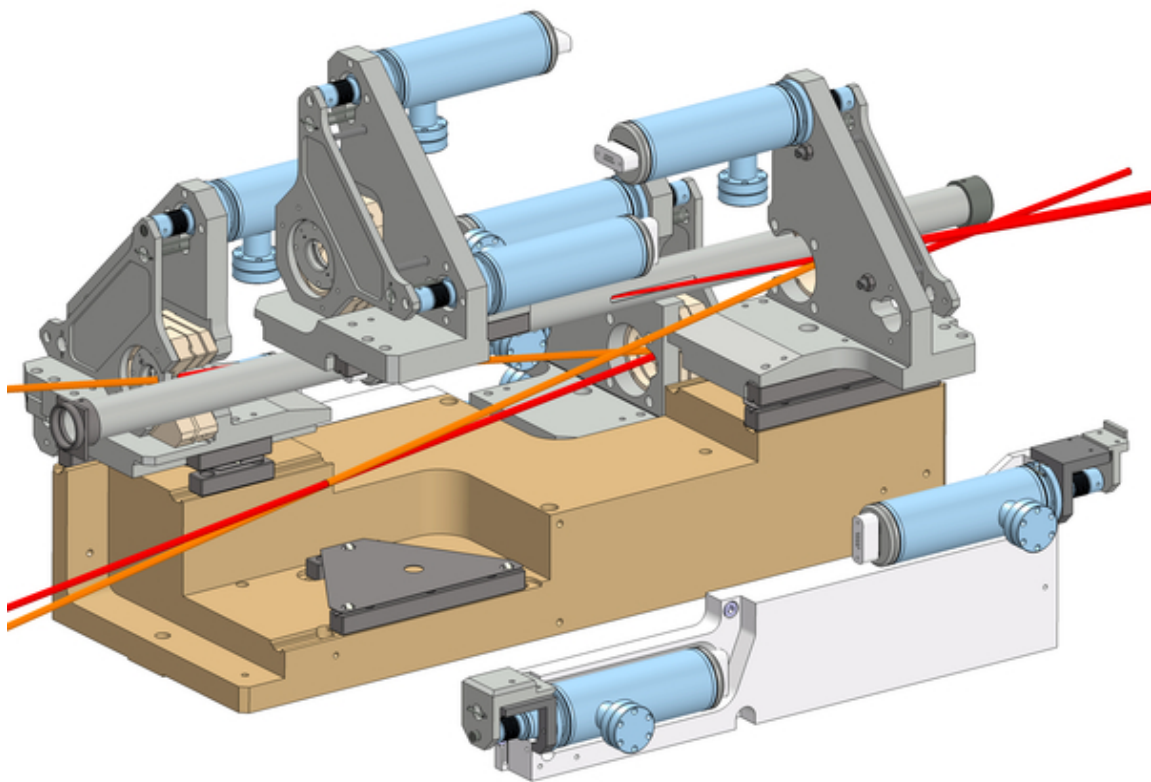


Figure 11. Exploded view of the four mirror mounts system. The invar plate with two encapsulated motors and one of the flat mirror mount system have been unlinked from the heavy stainless steel base for the drawing.

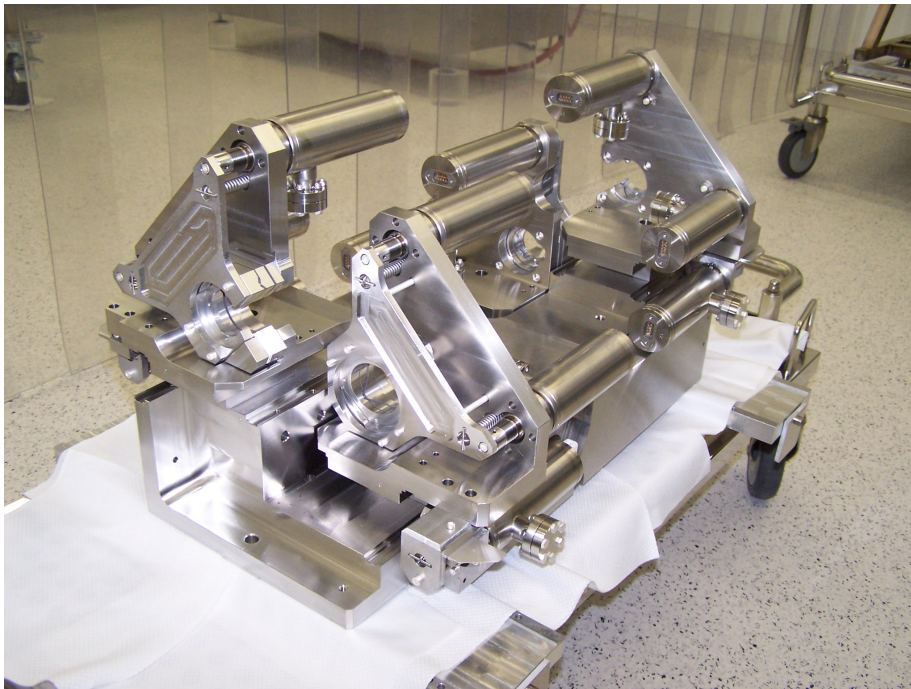


Figure 12. Picture of the four-mirror mounting system taken during the assembly in a clean class 10 (ISO4) room.

4. Fabry-Perot Cavity stabilization and the electronic system

Although the utmost care has been taken with the design, construction and assembly of the FPC this is not sufficient to reach the high level of stability required for a high gain in the cavity and to achieve collisions with the electrons circulating in the ATF damping ring. Therefore we have equipped our FPC with an active stabilization system. This active stabilization system performs several tasks. First of all it must ensure that the duration of a round trip for the photons circulating in the FPC has an integer relation with the time between two electrons bunches. The second task of the active stabilization system is to ensure that the laser pulses injected in the FPC arrive in time. The third task of this system is to have a slow control on the environmental variations. The overall architecture of the system is shown on figure 13.

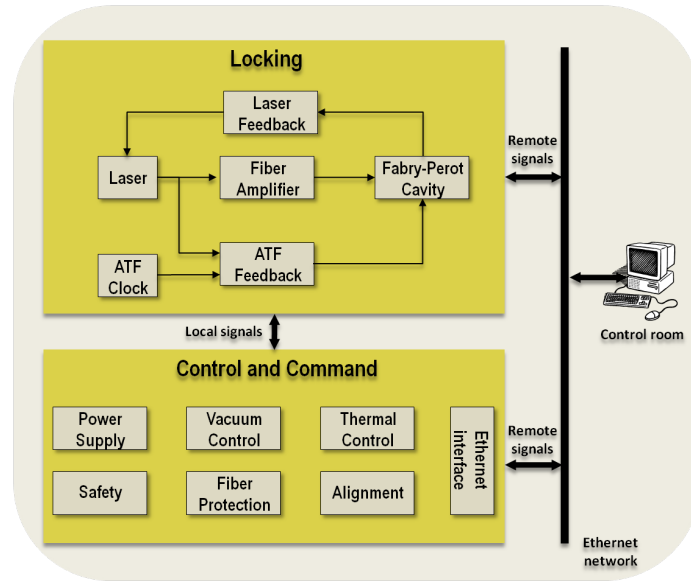


Figure 13. Overall architecture of the active stabilization system. The upper part is performed by the FPGA and the lower part is done by several remotely controlled sub-systems.

The first two tasks of the active stabilization system have to be performed at a very high speed to have a fast response time. We have therefore chosen to implement it on a VIRTEX-II FPGA (XILINX) commercial board VHS-V2-ADAC from Lyrtech. The overall board is shown on figure 14. This board is using several 14 bits ADC and DAC with a sampling speed of 60 megasample/s and clocked at 60 MHz. This board implements a double feedback system that synchronizes the FPC with the ATF clock and the laser oscillator with the FPC. The implementation of this double feedback system is shown on figure 15 and is detailed below. The other task of the active stabilization system, the correction of slow environmental variations, is performed by several sub-systems controlled remotely over the network by a desktop computer.

Ideally one would like the round trip of the photons in the FPC to be exactly equal to that of the electrons in the damping ring. However this would have required to match the length of the FPC to that of the damping ring, 154 meters, which would have been unpractical. Furthermore the ATF can operate in multibunch mode and in that mode bunches can be separated by 2.8 ns or a multiple

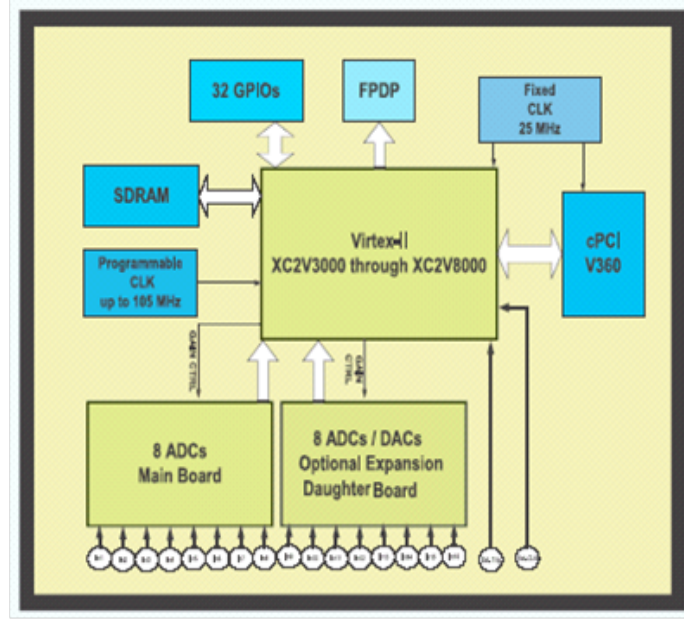


Figure 14. Lyrtech board architecture

of that value. As a round trip of 2.8 ns would have been impractically short, we choose to give our cavity a round trip of 5.6 ns (that is 1680 mm or 178.5 MHz). Given that the ATF has an harmonic number of 165 (i.e. it contains 165 RF buckets separated by 2.8 ns each), our photons perform 82.5 round trips in FPC while the electrons perform one round trip in the cavity. As a consequence a given electron bunch will collide with the photon pulse stored in the cavity on every other turn and during that time the photons will have done 165 round trips in the FPC. This is illustrated on figure 16.

Our system has to be able to work in the case where the two pulses (laser and electrons) are as short as about 20 ps every 5.6 ns, therefore the relative stability has to be around 10^{-3} , the natural stability of both systems allows us to use a feedback with a low bandwidth (about 100 Hz). Thus to lock the FPC round trip on the ATF clock we decided to act on the length of the FPC which has larger mirrors and thus are slower to react. For the other lock, the noise on the length difference between the FPC and the laser cavity has to be better than the wavelength over the finesse (the relative stability has to be around 10^{-10}), requiring a high feedback bandwidth and thus this loop acts on the mirrors of the laser cavity which are smaller.

4.1 FPC synchronization with the accelerator

A digital phase lock loop (PLL) is used to ensure that the round trip frequency in the FPC (178.5 MHz) keeps its integer relation with the round trip in the damping ring (2.165 MHz) with a very high accuracy (jitter of about 10 ps RMS). A synthesizer (AGILENT E8663B) locked to the ATF master clock is used to generate a 178.5 MHz reference signal. This reference signal is feed to an ADC where it is digitized with a sampling rate of 60 MHz. At this sampling rate the reference signal has a folded frequency of 1.5MHz ($178.5\text{MHz} - 3 \times 60\text{MHz}$). A photodiode located near the exit

KEK ATF-Laser-4M cavity Synchronization scheme

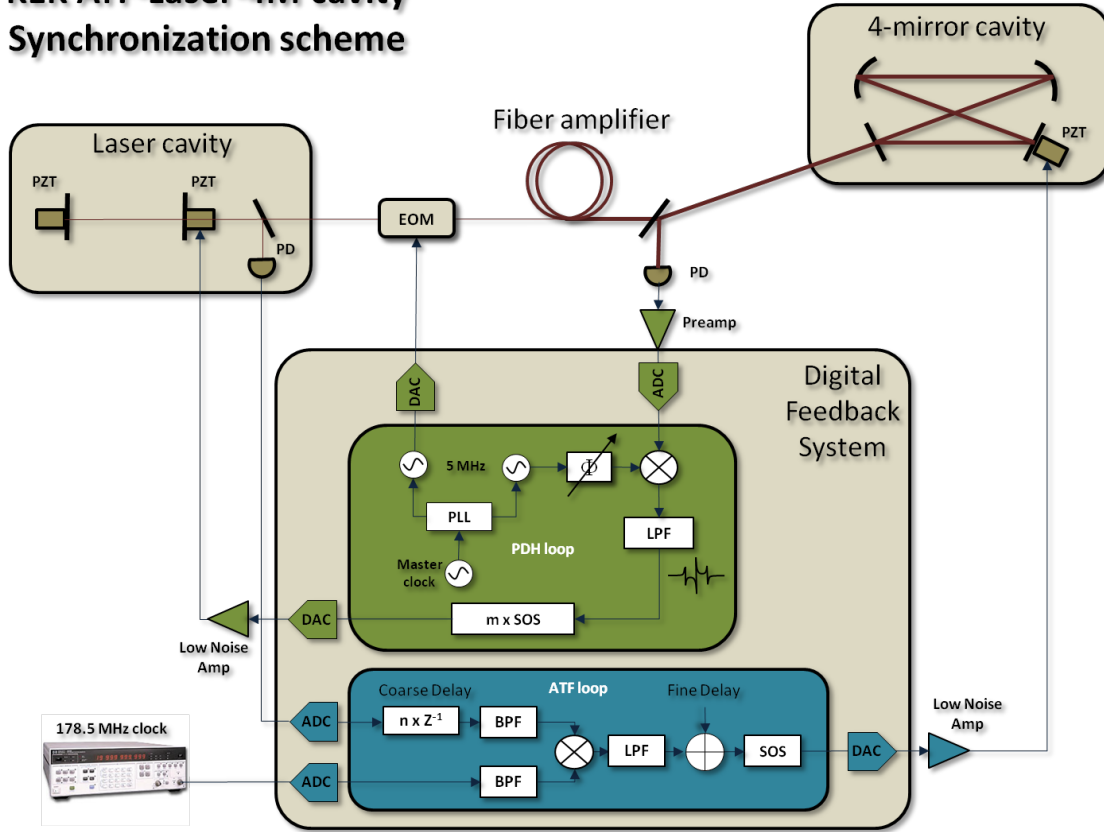


Figure 15. Implementation of the digital feedback system. The blue area is a digital phase lock-loop used to synchronize the FPC on the ATF clock. The signal produced by the feedback loop is used to adjust the length of the FPC by changing the tension applied on a PZT behind mirror M1. The green area is an implementation of the PDH technique to synchronize the laser oscillator on the FPC. When the photodiode located behind mirror M2 receives enough transmitted power the error signal produced using the PDH technique is used to vary the length of the laser oscillator cavity by acting on a PZT. All these features are implemented in a single FPGA board.

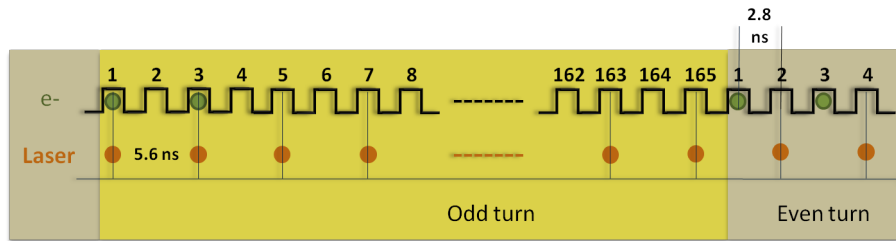


Figure 16. Time structure of the RF buckets (electron bunches) and of the laser, showing that collisions occur only every other turn.

of the laser oscillator is used to generate a second signal (see figures 2 and 15). This signal is also digitized at the same rate. These two digital signals pass through finite impulse response filters (FIR) acting as a band-pass filters. They are then mixed together. The resulting signal contains two components: one at high frequency (about 3 MHz) that is the sum of the two input frequencies and one at low frequency (near DC) that is the difference between these two frequencies. The high frequency component is removed by a digital low-pass filter and the remaining (low frequency) signal contains information on the frequency and phase difference between the two input signals. If the two signals were at the same frequency but at a different phase the resulting signal will be a simple DC offset whose value is proportional to the phase difference between the inputs. This signal is used to slightly move longitudinally mirror M2 in the FPC by varying the tension applied to a piezo-electric transducer (PZT) and therefore change the round trip (by 4.5nm/V) and the frequency of the FPC. This PZT has a low dynamic range and is used with a bandwidth of about 100 Hz. Additional displacements can be achieved thanks to motors located behind each mirror of the FPC. These motors allow changes in length of the FPC of the order of 25 mm, that is $\pm 130kHz$. This digital PLL is illustrated on the green part of figure 15.

Once the two signals are synchronized by the PLL their relative phase can be adjusted in a coarse manner by delaying the signal coming from the laser by a given number of FPGA clock cycles or in a fine manner by adding a given value to the output of the low-pass filter after the mixer.

The fact that the sampling frequency of the FPGA is lower than the frequency of the signals to be digitized is not a problem as both signal are almost at the same frequency and therefore the existence of phase and frequency differences between the two analog signals will lead to phase and frequency differences in the digitized signals. When the two signals have the same phase and frequency their digitized images are also similar and therefore no correction is applied to the FPC. We can ignore the risk of having the two signals being harmonic of each other when sampled at 60 MHz because this would result in a significant change in the length of the FPC or the damping ring (at least $60 \text{ MHz} \times c$) which are not physically possible.

4.2 Oscillator synchronization with the FPC

To ensure that the laser pulses are properly coupled to the FPC they must be injected at the correct time. To ensure this we use the Pound-Drever-Hall (PDH) technique [31] to adjust the length of the laser oscillator. The optical frequency stabilization must be better than the repetition rate over the Finesse (the FPC linewidth), which is 60 kHz. This is equivalent to a stabilization of the 1680 mm FPC length better than the laser wavelength over the finesse: 0.34 nm.

The natural stability of the laser oscillator is shown in figures 17 and 18.

As the PDH technique is described elsewhere in the literature [31] we only describe here its implementation in our setup. An electro-optics modulator (EOM) has been placed at the exit of the laser oscillator (see figure 2). This EOM is used to modulate the frequency of the laser pulses by $\pm 5MHz$. A photodiode is placed so as to see the part of the laser pulse that is reflected from the injection mirror M1. The signal from this photodiode is digitized by an ADC and then numerically demodulated in the FPGA (see figure 19). This signal (input frequency; IF) is then feed to a Finite Impulse Response filter (FIR), which has a band-pass frequency response. If the error is not too big the measured demodulated and filtered signal is directly proportional to the error on the injection

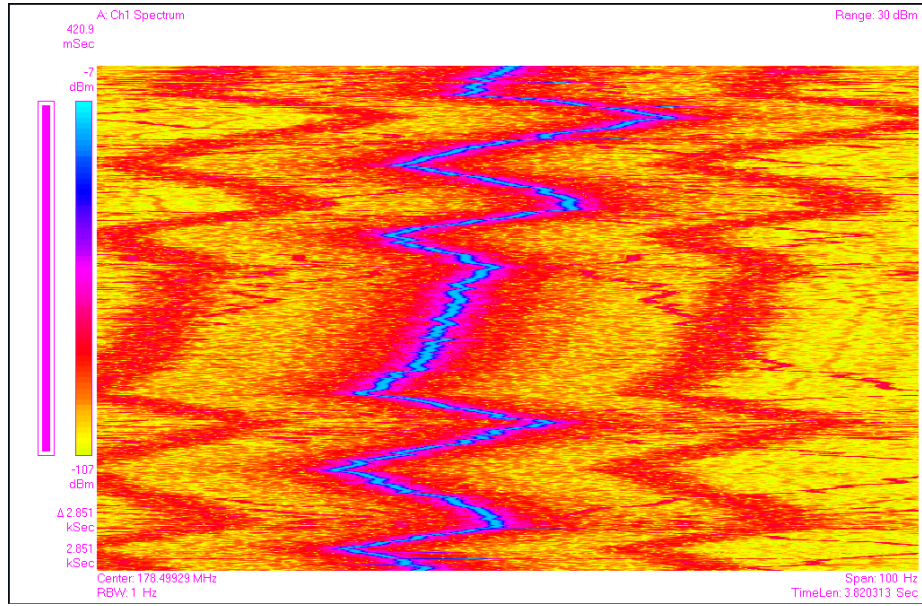


Figure 17. Long term stability drift of the OneFive Origami at 178.5MHz repetition rate. The horizontal axis is frequency offset (horizontal SPAN = 100 Hz) and the vertical axis is the measurement duration (47 minutes). The color of each pixel of this plot gives the power measured at the time and frequency indicated by the axis, red being the most intense. The red line on the plot shows the variation of the carrier frequency and the two light blue lines show that the sideband frequencies follow a similar pattern.

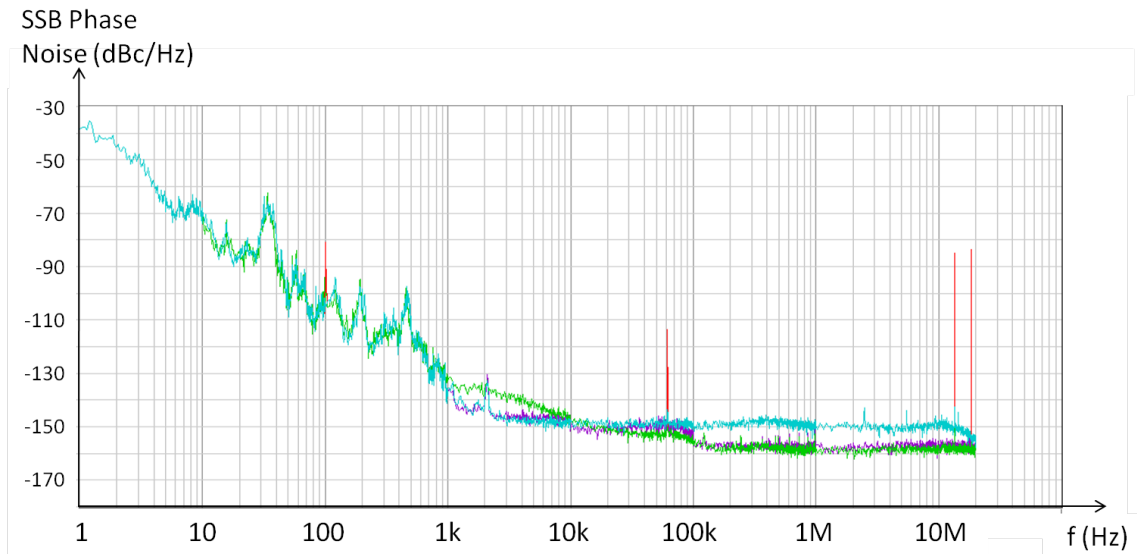


Figure 18. Phase noise power spectrum $L(f)$ ($F_{rep} = 178.5$ MHz) measured with different setup: internal InGaAs photodiode and 20dB amplifier (blue), external photodiode (Thorlabs DET10A/M; green) and external Hamamatsu InGaAs photodiode Hamamatsu and OneFive amplifier (red).

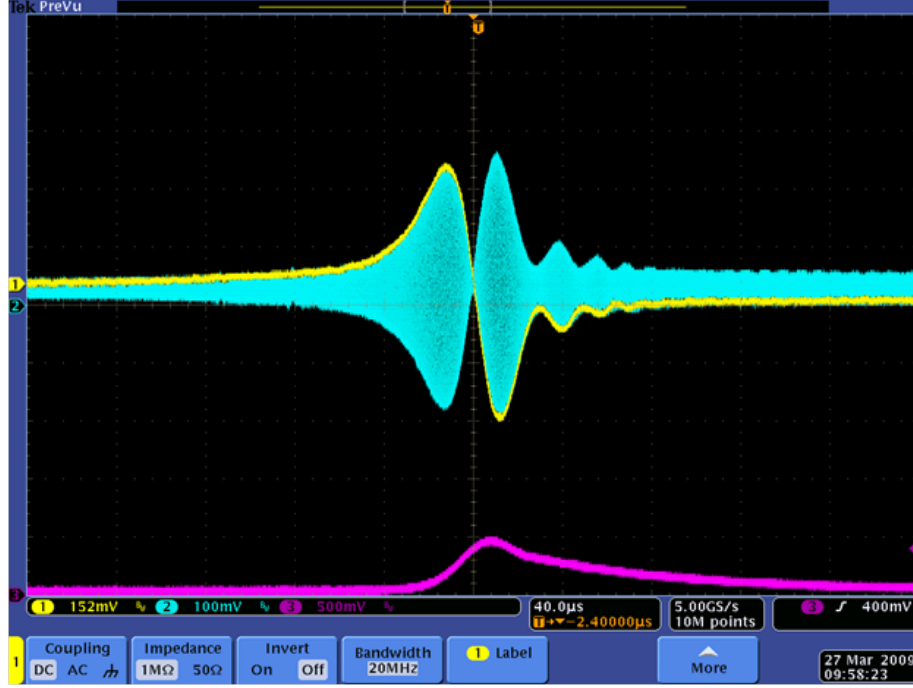


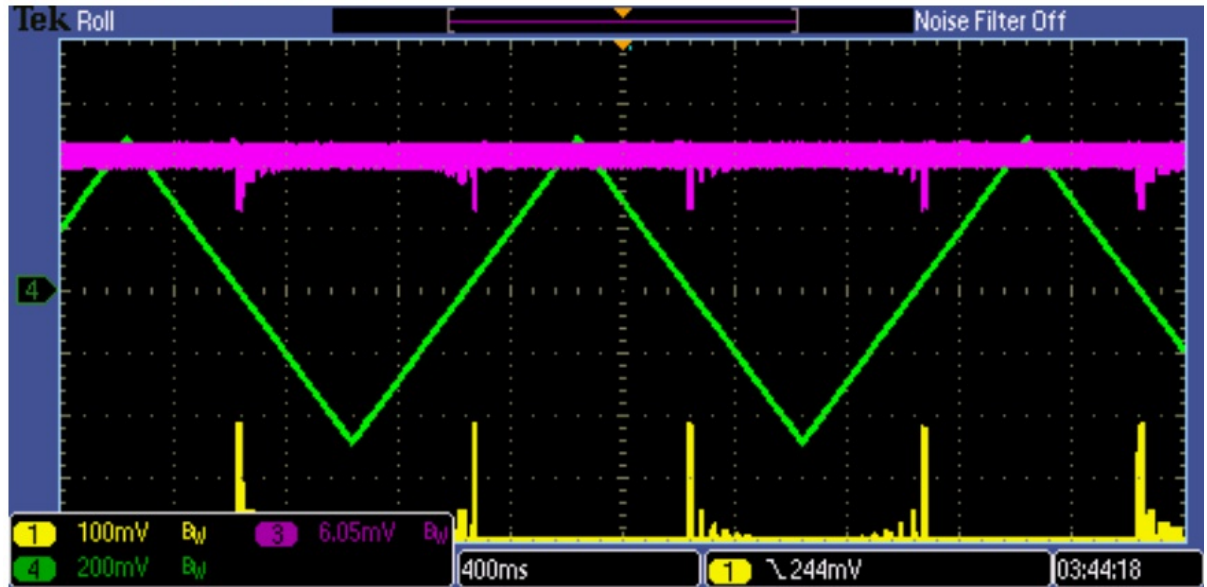
Figure 19. PDH error signal (blue) and IF signal (yellow) observed when the length of the FPC is varied with time. In the center one can clearly see the area where the error signal is linear. The purple line shows the power transmitted by the FPC.

time of the pulses in the FPC (see figure 19), however there is not enough bandwidth to act directly on the length of the FPC. Instead the error signal is used to drive a PZT located inside the laser oscillator. By acting on this PZT the length of the laser oscillator is changed so that the laser pulses are injected in the FPC with the proper timing and phase (see figure 15). As the PZT has a limited range the length of the laser oscillator can also be changed by larger steps by adjusting its temperature. This allows us to reach any frequency within a 8kHz range. To avoid changing the laser oscillator when no power is stored in the cavity and therefore the PDH error signal is not reliable a threshold is set on the minimum power that must be read by the photodiode located behind mirror M1 to allow actions on the laser oscillator PZT.

When no power is stored in the FPC the laser oscillator cavity length can be scanned by applying varying tension to the laser oscillator PZT. The range of this tension is adjusted manually around the values where we expect to see power accumulation in the FPC. An example of such scan is shown on figure 20 (top). Once the PZT scans the range where power accumulation occurs sufficiently slowly for the PDH error signal to be meaningful the system automatically switches to "locked" mode and uses the PDH error signal to vary the length of the laser oscillator as required to stay synchronized with the FPC. This is shown on the lower part of figure 20.

Although a great care has been taken while designing the feedback and selecting the components used to build it, it is necessary to construct a feedback filter which match the system's frequency response. It is therefore necessary to measure how the whole system (device and feedback) reacts to a given input and adjust it accordingly. This is done using an identification procedure [47].

Control: (20.10.66.99) Feb 21, 2011



Control: (20.10.66.99) Feb 21, 2011

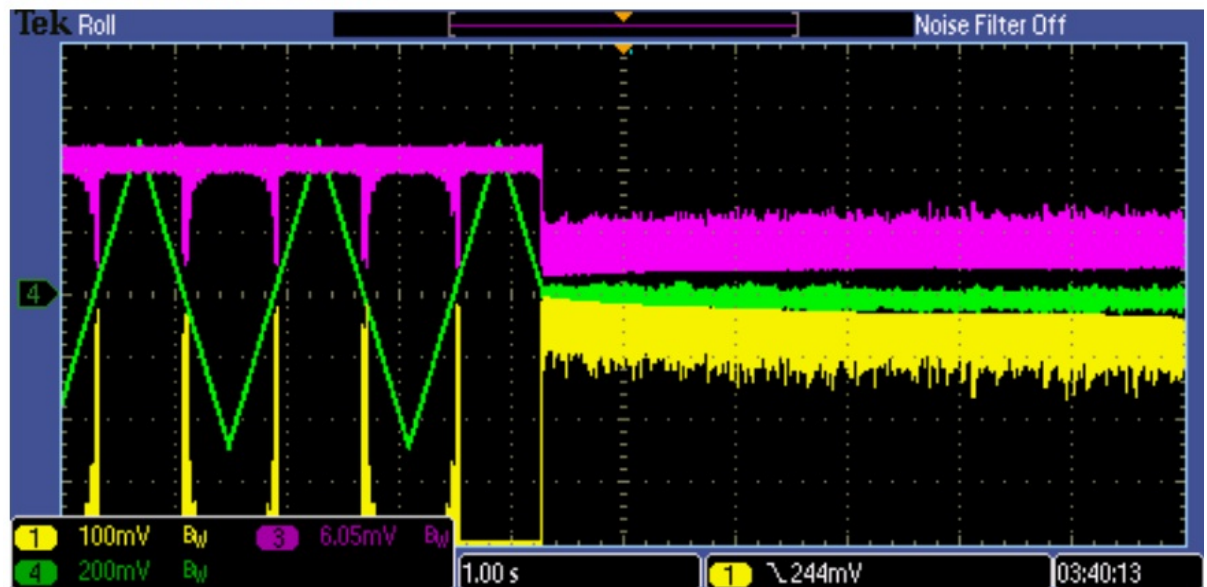


Figure 20. Oscilloscope traces showing the voltage applied to the PZT in the laser oscillator cavity (green), the power transmitted by the cavity (yellow) and the power reflected at the entrance of the cavity (magenta). To find the laser oscillator cavity length matching the FPC length we apply a triangular voltage on the PZT located in the laser oscillator cavity (upper plot). When the length of the laser oscillator becomes close a value that matches a mode in the FPC we see more power transmitted by the FPC (yellow) and less power reflected (magenta). If the power stored in the cavity becomes high enough to generate a usable PDH error signal the system automatically switches to that signal to adjust the laser oscillator cavity length (bottom plot).

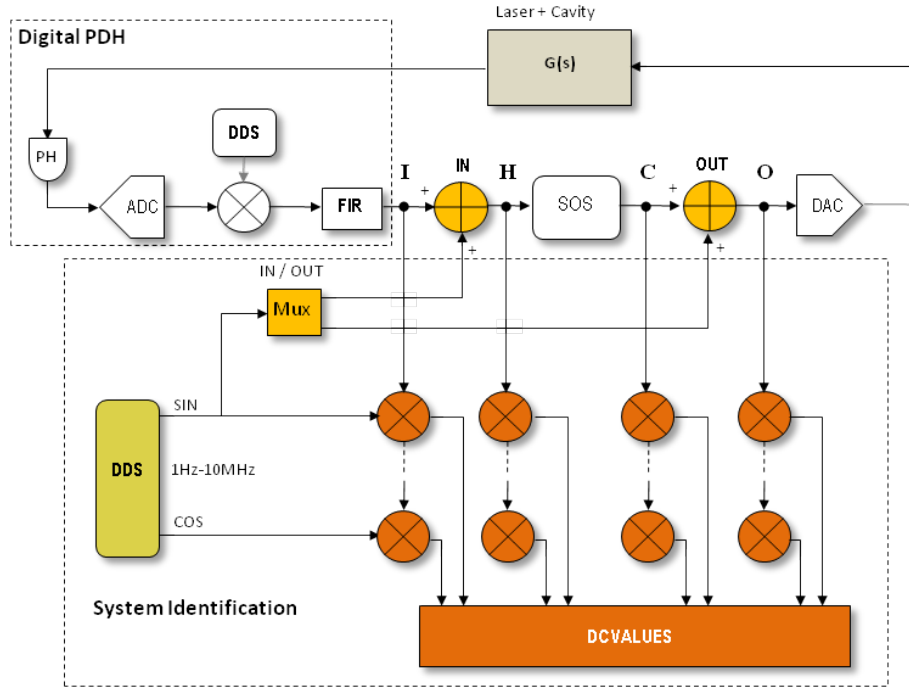


Figure 21. Block diagram of the laser oscillator to FPC feedback loop. To measure the response function of this feedback loop signal generated by the direct digital synthesizer (DDS) is injected in the loop before or after the SOS (locations "IN" or "OUT"). The response of the loop to this signal is read at locations I, H, C and O. The phase of this response is obtained by mixing it with the DDS signal. CHECK

The linear response of the system $y(z)$ can be described as follow [48]:

$$y(z) = G(z)u(z) + H(z)e(z) \quad (4.1)$$

$$u(z) = K(z)[r(z) - y(z)] \quad (4.2)$$

where z is the backward shift operator, $u(z)$ is the control input, $e(z)$ is white noise and $G(z)$ and $H(z)$ are the process transfer function, $K(z)$ is the feedback transfer function and $r(z)$ is the reference signal of the feedback.

Identification consists in estimating the parameters G and K by adding a known harmonic signal to the locked system and by making ratios between measured harmonic signals (see figure 21).

Practically this is done by injecting a known signal at various locations in our feedback loop and measuring the response of the various elements of the system. This has been fully implemented in the FPGA which is to our knowledge the first time it was done for such system.

Once the response of the system has been measured it is possible to adjust the digital filters in the FPGA to bring its response as close a possible for the desired response and to minimize the impact of resonances in the feedback loop.

Figure 22 shows the open loop Bode diagram obtained after performing such measurement. On this diagram the system's response has peaks beyond 10 kHz. This could also be seen by looking

directly at the power stored in the cavity on a scope (see figure 23 top). Using the knowledge gained by artificially stimulating our feedback system we modified the FPGA filters. After these modifications the power stored in the FPC was free of these resonances (see figure 23 bottom).

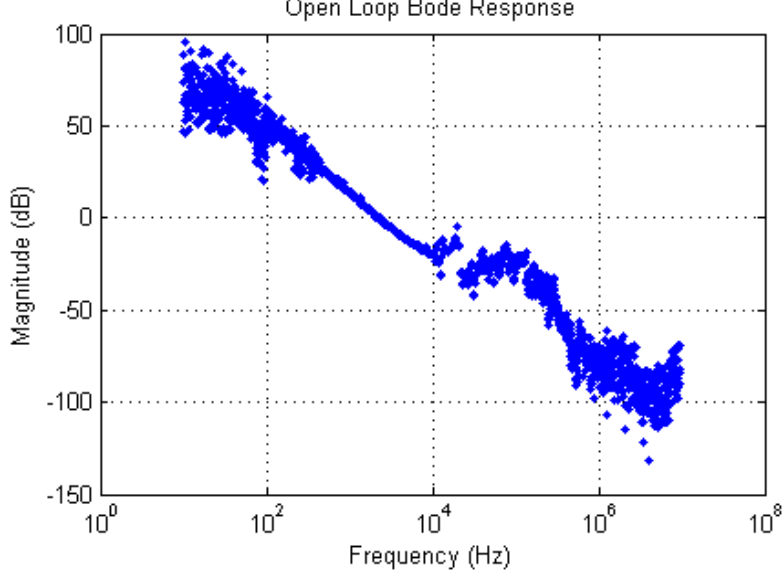


Figure 22. Bode diagram obtained by using the identification procedure to study the open loop response of our system. It can be seen that the system’s response is unstable above 20 kHz.

5. Performances and future developments

In this article, we described in details an apparatus, based on a non planar optical resonator, installed on the ATF electron ring. The system is meant to produce a circularly polarised high gamma flux from laser/ electron beam Compton scattering. This is the first time ever that a non-planar four mirrors cavity operating in pulsed mode and has been successfully deployed at an accelerator.

This apparatus has been installed at the KEK ATF during the summer 2010. The choice of a digital feedback made it easy to adapt it to the new system. Within weeks of installing the cavity we were able to perform several data taking run during which the two locks were kept during several hours (see figure 24). This has been validated experimentally by the observation of high energy gamma rays produced as soon as both the laser and the accelerator were operating. A flux of 2.7 ± 0.2 gamma rays per bunch crossing ($\sim 3 \times 10^6$ gammas per second) was achieved. The measurement of this flux and the analysis of the data taken is discussed in a companion paper [35].

For the commissioning, the cavity finesse was fixed to a moderate value of ≈ 3000 . A dedicated fiber based amplifier allowed us to reach ≈ 55 W of incident laser beam average power. The best laser coupling to the cavity was at most at 65%.

Before the earthquake that struck Japan in March 2011 we were working on several improvements to this system. To increase the power stored in the cavity, we intend to replace the current mirrors with higher reflectivity ones in order to achieve a finesse of 30 000. We also intend to

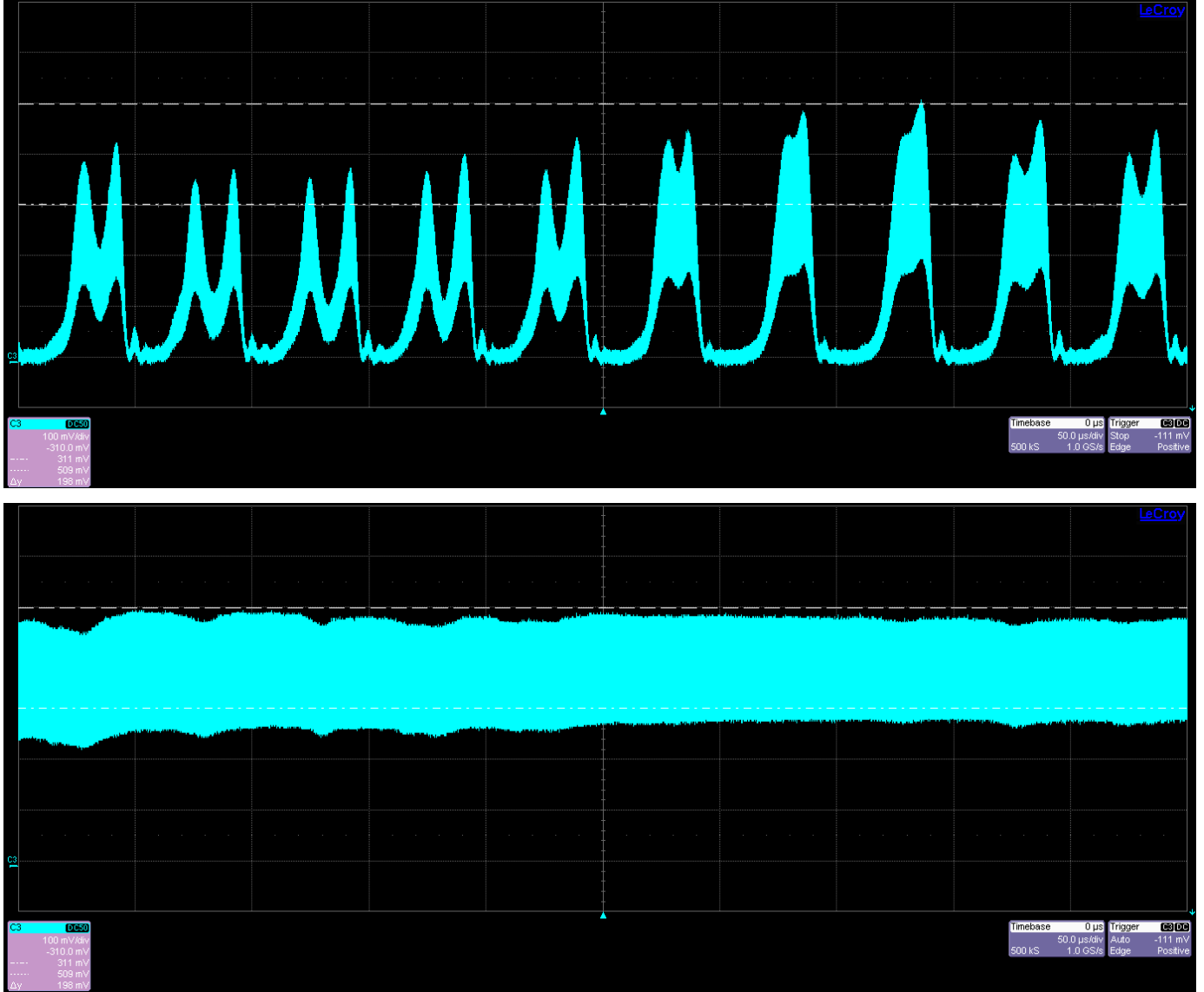


Figure 23. Example of power stored in the FPC before (top) and after (bottom) adjusting the filters. On the top plot resonances at 20 kHz and 40 kHz can clearly be seen. These resonances disappeared after the filters were adjusted. The power stored in the cavity is measured by placing a photodiode behind one of the mirrors of the FPC (in our case mirror M2).

improve the laser system and the injection optics to increase the power injected in the cavity. The great adaptability of the digital double feedback system gives us confidence that after increasing the cavity finesse we should still be able to lock.

The technology described in this article will be used to reach a final goal of 1MW average power stored inside a FPC with several possible applications.



Figure 24. Oscilloscope trace showing the voltage applied to the PZT in the laser oscillator cavity (green), the power transmitted by the cavity (yellow) and the power reflected at the entrance of the cavity (magenta). This trace shows the cavity locked during more than 20 seconds with a high level of stability.

Acknowledgements

This work has been funded thanks to a grant from the French ANR (Agence Nationale de la Recherche) under contract number BLAN08-1-382932 and P2I (Physique des 2 Infinis). The authors would like to thank the staff from KEK for their hospitality and their help with the design, the installation and the operation of this FPC. The authors are also grateful to Francois Richard for his continuous support.

References

- [1] P. Walter et al. A new high quality x-ray source for cultural heritage. *Comptes Rendus Physique*, 10(7):676 – 690, 2009.
- [2] Carroll F.E. Tunable monochromatic x rays: a new paradigm in medicine. *Am. J. Roentgenol.*, 179:583–590, 2002.
- [3] Biston M.-C. et al. Cure of fisher rats bearing radioresistant f98 glioma treated with cis-platinum and irradiated with monochromatic synchrotron x-rays. *Cancer Res.*, 64:2317–2323, 2004.
- [4] P. Suorti and W. Thomlinson. Medical applications of synchrotron radiation. *Phys. Med. Biol.*, 48:R1–R35, 2003.

- [5] Hajima R. et al. Proposal of nondestructive radionuclide assay using a high-flux gamma-ray source and nuclear resonance fluorescence. *J. Nucl. Sci. Technol.*, 45:441–451, 2008.
- [6] Albert F. et al. Isotope-specific detection of low-density materials with laser-based monoenergetic gamma-rays. *Opt. Lett.*, 35:354–356, 2010.
- [7] S. Araki et al. Design of a polarised positron source based on laser compton scattering. *Arxiv preprint physics/0509016*, 2005.
- [8] G. Moortgat-Pick et al. The Role of polarized positrons and electrons in revealing fundamental interactions at the linear collider. *Phys.Rept.*, 460:131–243, 2008.
- [9] G. Klemz, Klaus Monig, and I. Will. Design study of an optical cavity for a future photon-collider at ILC. *Nucl.Instrum.Meth.*, A564:212–224, 2006.
- [10] J. Urakawa. Development of a compact x-ray source based on compton scattering using a 1.3 ghz superconducting rf accelerating linac and a new laser storage cavity. *NIM A*, 637(1, Supplement 1):S47 – S50, 2011.
- [11] ThomX collaboration. Thomx cdr. *IN2P3*, in2p3-00448278, 2010.
- [12] Sprangle P. et al. Tunable, short pulse hard x-rays from compact laser synchrotron source. *Appl. Phys.*, 72:5032–5034, 1992.
- [13] E. Accomando et al. Physics at the CLIC multi-TeV linear collider. 2004.
- [14] James Brau, (Ed.) et al. ILC Reference Design Report Volume 1 - Executive Summary. 2007.
- [15] O. Dadoun et al. The Baseline Positron Production and Capture Scheme for CLIC. 1st International Particle Accelerator Conference: IPAC' 10, 23-28 May 2010, Kyoto, Japan.
- [16] Russbueldt P. et al. 400w yb:yag innoslab fs-amplifier. *Optics Expr.*, 17:12230–12245, 2009.
- [17] H. Kogelnick and T. Li. Laser beams and resonators. *Appl. Opt.*, 5:1550–1567, 1966.
- [18] Z. Huang and R. D. Ruth. Laser-electron storage ring. *Phys. Rev. Lett.*, 80(5):976–979, Feb 1998.
- [19] E. Bulyak et al. Compact x-ray source based on compton backscattering. *Nuclear Instruments and Methods in Physics Research Section A: Accelerators, Spectrometers, Detectors and Associated Equipment*, 487(3):241 – 248, 2002.
- [20] J. C. Diels R. J. Jones. Stabilisation of the frequency, phase, repetition rate of an ultrashort pulse train to a Fabry-Perot cavity. *Opt. Commun.*, 175:409–418, 2000.
- [21] Pupeza I. et al. Power scaling of a high-repetition-rate enhancement cavity. *Opt. Lett.*, 35:2252–2254, 2010.
- [22] Brisson V. et al. High finesse fabry-perot cavities in picosecond regime. *Nucl. Instr. Meth. A*, 608:S75–S77, 2009.
- [23] N. Falletto et al. Compton scattering off polarized electrons with a high finesse Fabry-Perot cavity at JLab. *Nucl.Instrum.Meth.*, A459:412–425, 2001.
- [24] S. Baudrand et al. A High Precision Fabry-Perot Cavity Polarimeter at HERA. *JINST*, 5:06005, 2010.
- [25] Sakaue K. et al. Observation of pulsed x-ray trains produced by laser-electron compton scatterings. *Rev. Sci. Instrum.*, 80:123304–123310, 2009.
- [26] S. Miyoshi et al. Photon generation by laser-Compton scattering at the KEK-ATF. *Nucl.Instrum.Meth.*, A623:576–578, 2010.

- [27] Zomer F. et al. Polarization induced instabilities in external four-mirror Fabry-Perot cavities. *Appl. Opt.*, 48:6651–6661, 2009.
- [28] F. Hinode et al. Atf accelerator test facility design and study report no. 4. *KEK, Tsukuba, Japan*, <http://lcdev.kek.jp/ATF/Pub/KEK-I-95-4.pdf>, 1995.
- [29] P. Bambade et al. Present status and first results of the final focus beam line at the kek accelerator test facility. *Phys. Rev. ST Accel. Beams*, 13(4):042801, Apr 2010.
- [30] Eidam T. et al. Femtosecond fiber CPA system emitting 830W average output power. *Opt. Lett.*, 35:94–96, 2010.
- [31] Drever W.P. et al. Laser phase and frequency stabilization using an optical resonator. *Appl. Phys. B*, 31:97–105, 1983.
- [32] Udem T. et al. Optical frequency metrology. *Nature*, 416:233, 2002.
- [33] Jones R.J. and Diels J.C. Stabilization of femtosecond lasers for optical frequency metrology and direct optical to radio frequency synthesis. *Phys. Rev. Lett.*, 86:3288–3291, 2001.
- [34] Jones R.J. et al. Precision stabilization of femtosecond lasers to high-finesse optical cavities. *Phys. Rev. A*, 69:051803, 2004.
- [35] Analysis of the data collected at a 4-mirror fabry-pérot cavity at the kek atf. *To be submitted*.
- [36] E. D. Black. An introduction to pound-drever-hall laser frequency stabilization. *American Journal of Physics*, 69(1):79, January January 2001.
- [37] Petersen J.C. and Luiten A.N. Short pulses in optical resonators. *Opt. Expr.*, 11:2975–2981, 2003.
- [38] Loewen R. A compact light source: Design and technical feasibility study of a laser-electron storage ring x-ray source. *Stanford University*, Ph.D. Thesis, 2003.
- [39] Kai-Hsiu Liao et al. Large-aperture chirped volume bragg grating based fiber cpa system. *Opt. Express*, 15(8):4876–4882, Apr 2007.
- [40] Hello P. Optical aspects in interferometric gravitational-wave detectors. *Progr. Opt.*, 38:85–164, 1998.
- [41] Arnaud J.A. and Kogelnik H. Gaussian light beam with general astigmatism. *Appl. Opt.*, 8:1687–1693, 1969.
- [42] Arnaud J.A. Nonorthogonal waveguides and resonators. *Bell Syst. Tech. J.*, 49:2311–2348, 1970.
- [43] Variola A. Luminosity optimization schemes in Compton experiments based on Fabry-Perot optical resonators. *Phys. Rev. ST AB*, 14:031001, 2011.
- [44] Fedala Y. Etude d’une cavité fabry pérot haute finesse à quatre miroirs pour des applications de production de rayons x et gamma par interaction compton laser-électrons. *Université de Paris-Sud XI, Laboratoire de l’Accélérateur Linéaire*, Thèse de doctorat, 2008.
- [45] Y. Honda et al. Stabilization of a non-planar optical cavity using its polarization property. *Optics Communications*, 282(15):3108 – 3112, 2009.
- [46] H. Sakai et al. Measurement of a small vertical emittance with a laser wire beam profile monitor. *Phys. Rev. ST Accel. Beams*, 5:122801, Dec 2002.
- [47] M. Gevers et al. Identifiability and informative experiments in open and closed-loop identification. In Alessandro Chiuso, Stefano Pinzoni, and Augusto Ferrante, editors, *Modeling, Estimation and Control*, volume 364 of *Lecture Notes in Control and Information Sciences*, pages 151–170. Springer Berlin / Heidelberg, 2007. 10.1007/978-3-540-73570-0_13.

- [48] A. Esmaili, J. F. MacGregor, and P. A. Taylor. Direct and two-step methods for closed-loop identification: a comparison of asymptotic and finite data set performance. *Journal of Process Control*, 10(6):525 – 537, 2000.